Fabrication of Fully Inkjet-Printed Vias and SIW Structures on Thick Polymer Substrates

Sangkil Kim, Atif Shamim, Apostolos Georgiadis, Hervé Aubert, Manos M. Tentzeris

Fabrication of Fully Inkjet-Printed Vias and SIW Structures on Thick Polymer Substrates

Sangkil Kim, *Member, IEEE*, Atif Shamim, *Senior Member, IEEE*, Apostolos Georgiadis, *Senior Member, IEEE*, Hervé Aubert, *Senior Member, IEEE*, and Manos M. Tentzeris, *Fellow, IEEE*

***Abstract*—In this paper, a novel fully inkjet-printed via fabrication technology and various inkjet-printed substrate integrated waveguide (SIW) structures on thick polymer substrates are presented. The electrical properties of PMMA are thoroughly studied up to 8 GHz utilizing the T-resonator method, and inkjet-printable silver nanoparticle ink on PMMA are characterized. A "long via" fabrication process up to 1 mm utilizing inkjet printing technology is demonstrated and its characteristics are presented for the first time. The inkjet-printed vias on 0.8 mm thick substrate have a resistance of about 0.2 Ω. An equivalent circuit model of the inkjet-printed stepped vias is also discussed. An inkjet-printed microstrip-to-SIW interconnect and a SIW cavity resonator utilizing the proposed inkjet-printed via fabrication process are also presented. The design of the components and the fabrication steps are discussed, and the measured performances over the microwave frequency range of the prototypes are presented.**

***Index Terms*—Additive fabrication, inkjet-printed Substrate Integrated Waveguide (SIW), inkjet-printed via, low-cost via fabrication, Polymethyl methacrylate (PMMA).**

I. Introduction

INKJET printing technology is investigated and widely utilized as an alternative fabrication method to the conventional subtractive fabrication methods, such as milling and etching. The importance of "green", scalable and cost-efficient technology is ever increasing for numerous applications like the Internet of Things (IoT), the radio frequency identification tags (RFIDs), and the wireless sensor networks (WSNs) [1-3]. The inkjet printing technology does not produce any byproducts because it only deposits the controlled amount of functionalized inks such as silver nanoparticles on desired position. In addition, it is a completely dry process which is compatible with most modern fabrication processes [4]. Arbitrary geometries with small feature sizes (less than 50 µm) can be printed on numerous substrates without any special masking [5-7]. Recently, the development of various types of nanoparticle-based inks such as polymers, carbon nanotubes (CNTs), piezoelectric materials, and high dielectric constant materials has attracted significant interest from many researchers [8-11]. Numerous studies and applications utilizing inkjet printing technology in microwave area have been reported including inkjet-printed wireless power transfer topologies, RFID-based sensors and microwave components for high-speed communication systems [12,13]. However, most of these works are single-layered structures because it is challenging to realize inkjet-printed vias, which are one of the most critical factors for the realization of highly integrated systems, packages and multi-layered structures.

In this work, the implementation of inkjet-printed stepped vias on thick substrates (thickness > 100 µm) is presented for the first time. Only a small number of technologies for implementing vias utilizing inkjet printing technology have been reported, all of which have been implemented on thin substrates with thickness below 100 µm [14-18]. Such thin substrates are unsuitable for applications in relatively lower frequency bands, such as mobile, WiFi, ISM, etc. The feature size of microwave components, such as the width of microstrip line, is narrow on thin substrate, which results in high design sensitivities to fabrication tolerances. On the other side, the radiation efficiency of antennas, like patches, resonators and waveguide structures (such as substrate-integrated waveguides (SIW)) is significantly affected by the substrate thickness [19]. Therefore, it is necessary to develop via fabrication concepts or techniques which can be applied to various substrates of different thicknesses. The major issue in the metallization of via holes utilizing inkjet printing technology is to maintain a continuous and uniform metal layer since the printed traces shrink after the sintering process, which is challenging because the inkjet-printed silver nanoparticles shrink during sintering process. Cylindrical copper pillars were inserted in laser drilled via holes to metalize the thick via holes [20]. High conductivity and thick metal thickness compared with those of the printed nanoparticle-based metallic layers can be achieved by using this technology since thick copper pillars are utilized. However, it has limited design degrees of freedom because the size of copper pillar (*i.e.* length, radius, etc.) is fixed and additional soldering process is required to ensure the contact between planar metallic layers and the copper vias.

In this work, a novel via hole topology with an exponentially tapered profile is introduced in order to facilitate the formation of continuous metal layers using conductive inks. As a proof-of-concept demonstration of the proposed inkjet-printed stepped via configuration, an equivalent circuit model and a SIW structure, such as a microstrip-to-SIW transition, are presented on the polymethyl methacrylate (PMMA) substrate. A via array and a SIW cavity resonator are also presented on RT/Duroid 5880 to verify the repeatability of via fabrication process and its performance. SIW structures require a large number of vias, which makes them good benchmarking structures to test the repeatability and performance of the proposed stepped vias. PMMA, which is also known as Plexiglas or acrylic, is a widely used commercial polymer

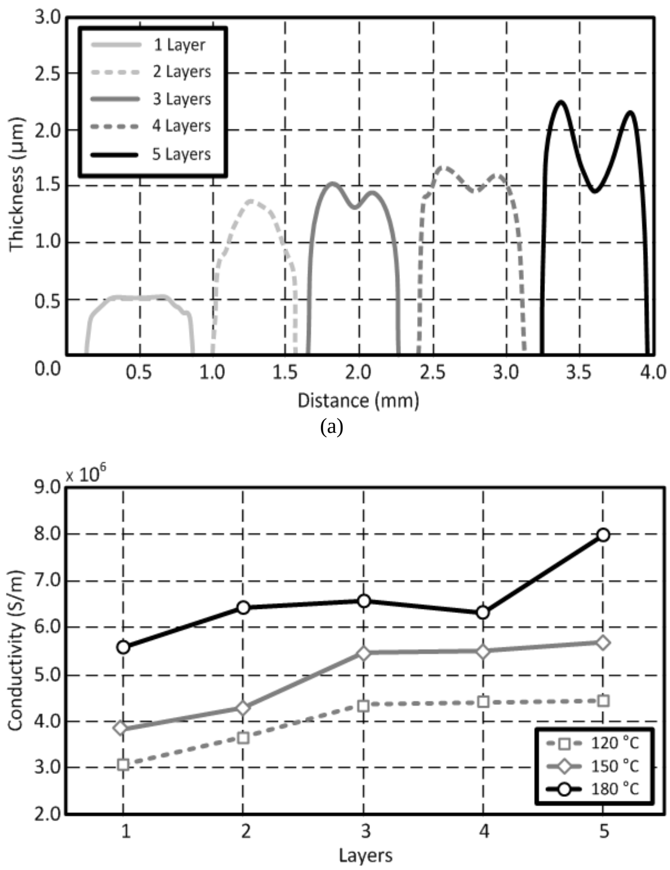

(a)

(b)

Fig. 1. Thickness and conductivity of inkjet-printed traces: (a) thickness (b) conductivity.

material for numerous applications such as display devices and medical instruments due to its high transparency and good compatibility with human tissues [21]. However, the electrical properties of PMMA at microwave frequency range as well as the characteristics of inkjet-printed silver nanoparticles on PMMA are not well known. Therefore, PMMA is chosen as a substrate, and its electrical properties are characterized for the first time in this work. In addition, the demonstration of the first fully inkjet-printed SIW structures suggests the importance of inkjet-printing technology toward implementing the system-on-substrate (SoS) concept in communication, sensing and Internet of Things (IoT) applications [13,19].

In Section II, the characterization of PMMA and inkjet-printed silver nanoparticles on PMMA is presented, while in Section III, the fabrication process of inkjet-printed stepped via is introduced. Section IV introduces the first fully inkjet-printed SIW structures including a SIW cavity resonator and a microstrip-to-SIW transition.

II. Inkjet Printing Process on PMMA Substrate

PMMA was chosen as the substrate for the realization of the via-enabled structures in this work because its electrical properties at microwave frequency range were not clearly reported although it is widely utilized for microwave applications, such as in microfluidic sensors. A thorough characterization of inkjet-printed silver nanoparticles on PMMA is necessary in order to extend the capabilities of inkjet-printed technologies to include via metallization and fabrication of SIW topologies.

In this section, the properties (conductivity, thickness) of inkjet-printed conductive traces using silver nanoparticles on PMMA substrate are investigated, while the electrical properties of PMMA are characterized within microwave frequency range (1 ~ 8 GHz) utilizing the T-resonator method [22].

A. Inkjet-printed Silver Nanoparticles on PMMA

The properties of inkjet-printed silver nanoparticles have different values depending on the substrate properties. It is because different substrates have different physical surface properties such as roughness, surface energy, and contact angle with the ink, that result in different inkjet-printability and printing challenges [23].

Simple rectangular traces (0.5 mm × 5 mm) were printed on PMMA substrate (Goodfellow, London, UK [24]) in order to investigate the properties of inkjet-printed silver nanoparticles on PMMA. The DMP2800 inkjet printer was utilized to print silver nanoparticles in this work. For printing, the Dimatix 10 pL cartridge (DMC-11610) was used, and it was kept at a distance of 250 μm from the surface of the substrate. The printer head angle was 4.5˚ which achieves a printing resolution of 1270 dpi (dots per inch). Cabot conductive ink CCI-300 was jetted at a nozzle temperature of 36 °C, while the substrate was maintained at room temperature (25 °C). Fig. 1(a) shows the thickness of the printed silver nanoparticle-based lines depending on the number of printed layers. The printed patterns were sintered at 120 ˚C for 2 hours, and the thickness was measured using a Veeco Dektak 150 surface profilometer. Each printed layer added about 500 nm of thickness to the printed traces. A reported minimum feature size of the silver nanoparticle ink using a commercially available printer is about 50 μm up to 5 layers of printing. After printing the third layer, the coffee ring effect has been observed because of the high surface energy of PMMA. The high surface energy of PMMA results in different drying speeds of ink at the edge and middle of the printed patterns [25,26]. The width of the printed trace is additionally increased by about 80 μm for each additional printed layer when the thickness (height) of the printed traces has exceeded 1.5 μm. The inkjet printing technology is a thin metal process that thickness of printed traces, such as metals and polymers, is about one skin depth or less at the microwave frequency range. However, it takes advantage of flexibility, ease of fabrication, and cost efficiency of the printing technology which are critical properties for implementing novel applications, such as IoT. The conductivity (σ) of the inkjet-printed silver nanoparticles was also extracted using the measured profiles of the printed traces using Eqs. (1),

$$\sigma = \frac{l}{R \cdot A} \text{ (S/m)} \tag{1}$$

where l is the length of the trace, R is the resistance across the trace, and A is the cross-section area of trace. The cross-section areas of the printed traces were numerically integrated over the line width (Fig. 1(a)). Fig. 1(b) shows the extracted

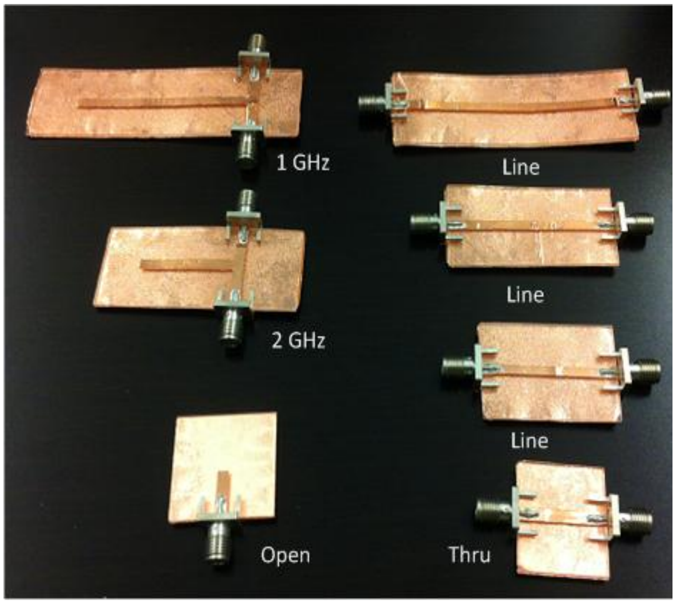

Fig. 2. Fabricated T-resonators and TRL calibration lines on PMMA substrate

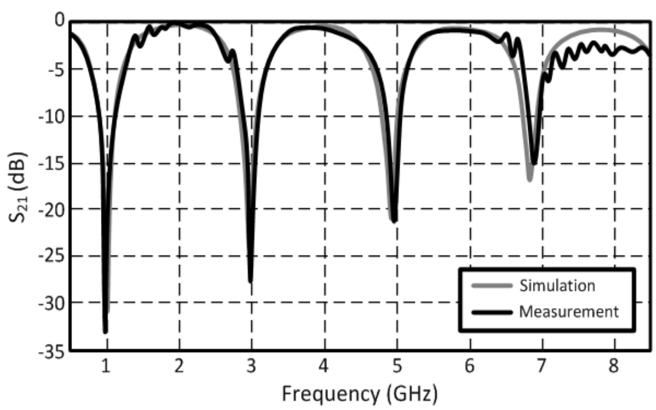

Fig. 3. S_{21} of the 1 GHz T-resonator.

conductivities for different sintering temperatures as a function of the number of printed layers. The conductivity value converges after printing 3 layers because the particle density is saturated. Higher sintering temperatures resulted in higher conductivity values as reported in previous studies [13,27]. The converged conductivity values of the silver nanoparticle ink were around 4.4×10^6 S/m at 120 ˚C, 5.7×10^6 S/m at 150 ˚C, and 6.9×10^6 S/m at 180 ˚C. It corresponds to 6.98 %, 9.05 %, and 10.95 % of bulk silver's conductivity ($\sigma_{\mathrm{Ag}} = 6.3\times10^7$ S/m), respectively.

B. RF Characterization of PMMA

A commercially available PMMA sample has been characterized up to 8 GHz through the microstrip T-resonator method in this work. The relative permittivity (ε_r) and loss tangent (tan δ) have been extracted from the measurements. Fig. 2 shows the fabricated T-resonator structures and the thru-reflection-line (TRL) calibration structures on 1 mm thick PMMA. The T-resonators consist of 50 Ω feeding lines and an open stub. The length of the open stub is quarter-wavelength (λ_g/4) at the desired resonant frequency. The width of the microstrip feeding lines was 2.8 mm and the length of the T-resonator for 1 GHz is 51.92 mm and for 2 GHz is 25.56 mm. Fig. 3 shows the measured S_{21} of the fabricated T-resonator for 1 GHz. The measurement and simulation results are in good agreement. The resonant frequencies (f_n) of the T-resonator can be determined by Eqs. (2)

$$f_n = \frac{n\cdot c}{4(L_{phy}+L_O-L_T)\sqrt{\varepsilon_{eff}}} \tag{2}$$

where n is the odd resonance mode order (n = 1, 3, 5 ...), c is the speed of light in free space, L_{phy} is the physical length of the open stub, L_O is the correction factor for the open-end effect of the open stub, L_T is the correction factor for the T-junction effect, and ε_{eff} is the relative effective permittivity [22].

The loss tangent (tan δ) of the PMMA substrate was extracted from the quality factor (Q) of each resonance as reported in [22]. The conductor losses were theoretically estimated using equations reported in [30], and radiation losses were also theoretically calculated utilizing 3D full wave simulator, ANSYS HFSS v11.1.1. A thin copper sheet (thickness = 100 µm, $\sigma = 5.8\times10^7$ S/m) was utilized as the metal layer.

The coaxial SMA connectors were mounted using a conductive silver epoxy and TRL calibration was applied to de-embed the effects of feeding lines and the SMA connectors. The extracted effective permittivity (ε_{eff}) was converted to relative permittivity (ε_r). The resulting relative permittivity (ε_r) was 2.38 ± 0.12 and the extracted tan δ was 0.011 ± 0.002 over the frequency of 1 ~ 8 GHz band as shown in Fig.4. The error intervals were estimated for a 99 % confidence interval. Characterization results using the two-line-method are included in Fig. 4 for validation purpose [32]. Two transmission lines with the same characteristic impedance and two different lengths (20 mm and 70 mm) were prepared on the same substrate and their scattering parameters (S_{21}) were measured. The lengths of the transmission lines were corresponding to effective electrical length of 30° and 100° at 1 GHz, respectively. These transmission lines were utilized as the delay lines for TRL calibration. The relative dielectric constants (ε_r) over the frequency range of operation were extracted from the phase difference of the test transmission lines and the tan δ over the frequency were calculated from the attenuation constant (α) of the transmission lines. The calculated radiation loss using 3D EM simulator of the transmission line was subtracted from the measurement. These results are in good agreement and support the extracted values from the T-resonator method. The extracted dielectric constant values from the T-resonators vary compared to the values from the transmission line method. It is because of fabrication error of each resonator since the T-resonators were cut out from a copper tape. However, the extracted values from each resonators, such as a T-resonator for 1 GHz (resonant frequencies: 1 GHz, 3 GHz, 5 GHz, and 7 GHz), are robust over the frequency band.

III. Inkjet-printed Via

In this section, a novel via fabrication process on thick substrates utilizing inkjet printing technology is presented. In previously reported research efforts, inkjet-printed via holes

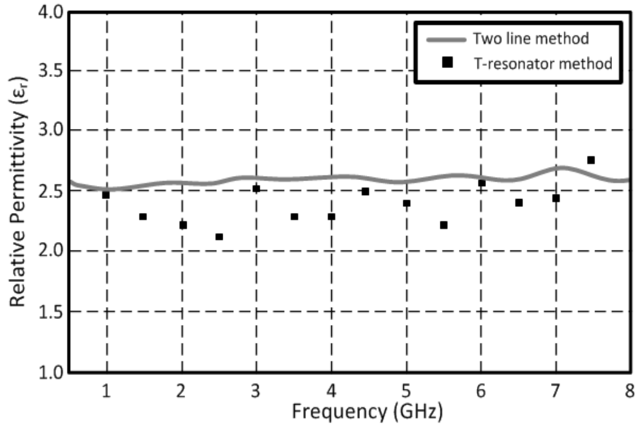

(a)

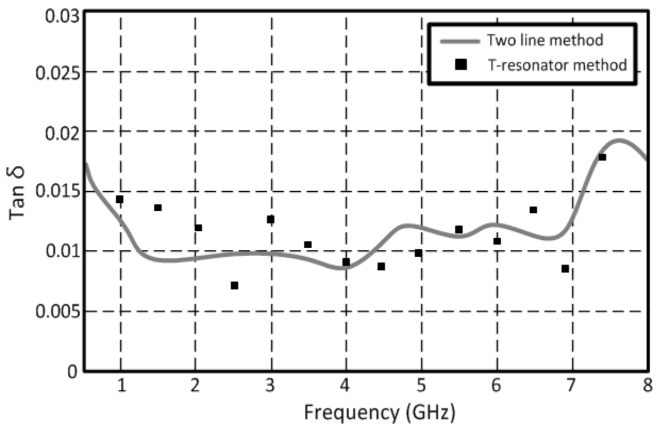

(b)

Fig. 4. Extracted (a) relative permittivity (ε_r) (b) loss tangent (tan δ)

TABLE I
VIA COMPARISON

	Via thickness (µm)	Via diameter (µm)	Resistance (Ω)
[14]	25 ~ 65	N/A	1.9 ± 0.1
[15]	0.5	0.75	5×10^5
[16]	100	65	0.52
[17][18]	50 ~ 80	N/A	0.073 ± 0.043
Proposed Structure	800 ~ 1000	2000	0.2

have been successfully implemented on thin substrates [14-18], as shown in Table I. In [14], 3 layers of silver nanoparticles have been printed over a thin vertical wall utilizing 50 pL cartridge. In [15], a crater-like via hole is made by inkjet printing an ethanol drop to dissolve a polyvinyl phenol (PVP) layer. In [16], a micro-via array, which consists of small laser-drilled micro-vias, is presented on polyimide substrate. In [17] and [18], printed microwave structures, such as microstrip lines, are presented, and the reported loss of printed microstrip lines are about 0.3 ~ 0.5 dB/mm up to 10 GHz. The reported printed vias shown in [14] ~ [18] are built on a thin substrate which thickness is less than 100 µm. The proposed stepped via approach (with a 2 mm diameter) achieved the via thickness of 800 ~ 1000 µm with a good via resistance of 0.2 Ω compared to the reported works.

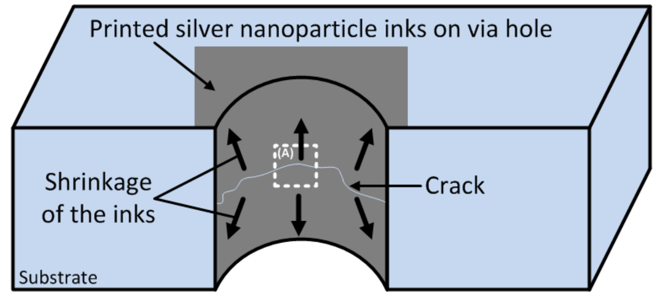

(a)

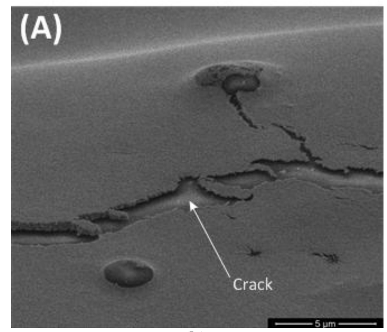

(b)

Fig. 5. (a) Crack formation of inkjet-printed silver nanoparticle on a straight vertical via hole and (b) SEM image of the crack on the metalized via hole.

It is challenging to metalize via holes on relatively thick substrates. If the via holes are metalized with a similar approach to other inkjet-printed structures, i.e. printing multiple layers on drilled via holes, it results in discontinuities, as shown in Fig. 5. For demonstration purposes, a straight via hole was drilled on 1 mm thick PMMA using CO_2 laser, and silver nanoparticles were printed over the via hole 5 times. The printed via hole was sintered at 120 ˚C for an 1 hour. The printed silver nanoparticles failed to form a continuous metal layer on the via hole because of the shrinkage of the silver ink during the sintering process due to the evaporation of the solvents, the polymers (a dispersant on the silver nanoparticles) and the impurities of the ink. The gravity force further enhances the downward shrinkage of the ink, which results in cracks on the metalized via wall. The shrinkage of the inkjet-printed silver nanoparticles on the vertical via wall is briefly depicted in Fig. 5(a). The inkjet-printed silver nanoparticles on the vertical wall are shrinking in different directions, and these results in cracks as shown in Fig. 5(b).

A novel stepped via hole topology is introduced in order to create a gradual transition between the top and the bottom planar substrate surfaces and reduce the stress on printed silver nanoparticles on the via hole during the sintering process. The fabrication process is described in Fig. 6. A thin concentric circular cylinder is engraved on the substrate to form a stepped via profile (Fig. 6(a)-(i), (ii)). Then, the substrate is flipped to drill another stepped via on the bottom side (Fig. 6(a)-(iii), (iv)). It is necessary to form a smooth transition from the via top to the bottom of the substrate. The final step is the inkjet printing process (Fig. 6(a)-(v), (vi)). The

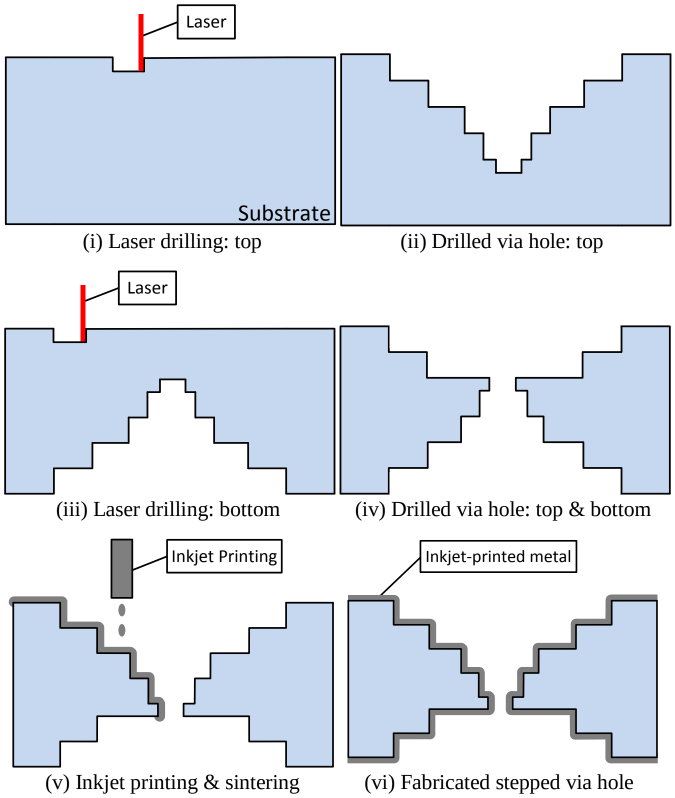

(a)

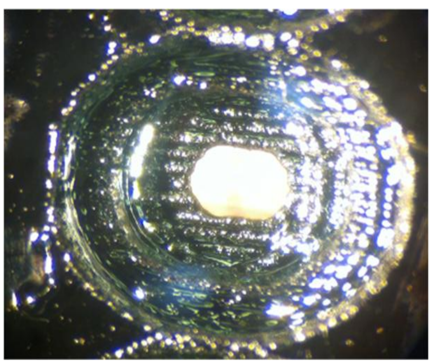

(b)

Fig. 6. (a) Stepped via hole fabrication process (b) fabricated stepped via hole (magnification ratio: x10)

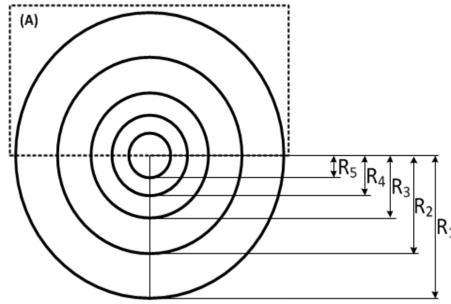

Radius	Value (mm)
R_1	1.00
R_2	0.63
R_3	0.40
R_4	0.25
R_5	0.16

(a)

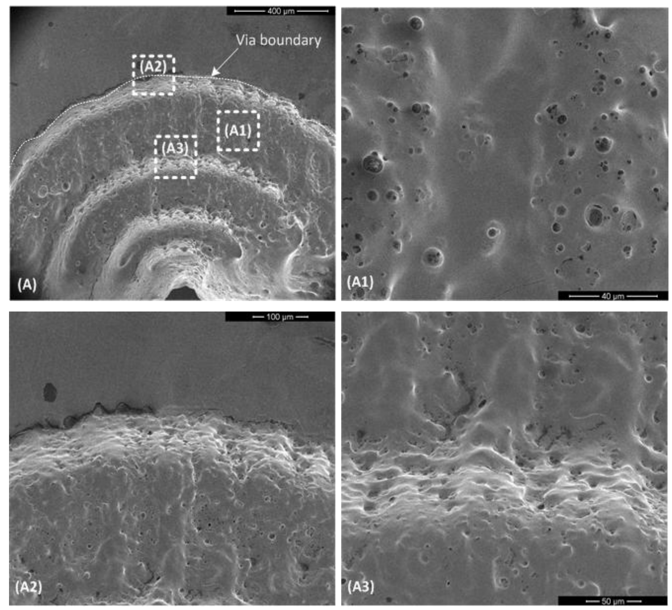

(b)

Fig. 7. (a) Geometry of stepped via hole and (b) SEM images of metalized stepped via hole: top view

fabricated stepped via hole on PMMA is shown in Fig. 6(b). This fabrication process is suitable for the inkjet printing because the drilling process and inkjet printing process are completely separate, while the via metallization is easily achieved during the inkjet printing (totally dry) process without any additional steps. The fabrication concept shown here on PMMA substrate is for proof of concept only, and is equally applicable to any other inkjet printable substrates.

The fabricated inkjet-printed vias are shown in Fig. 7 and Fig. 8. The geometries of the stepped via (top and side views) are shown in Fig. 7(a) and Fig. 8(a). Five concentric disks were drilled to form a stepped via profile on the top and two concentric disks were drilled on the bottom. A symmetric via profile (the same number of disks on the top and the bottom) requires precise control of the laser power level and alignment to match each end of the drilled stepped via topology which is more significantly challenging than the asymmetric stepped via topology. The ratio of the drilled disks is kept to the same value. The two concentric disks on the bottom with gradually increasing radii make sure that the penetration of the via hole runs through the entire substrate, because the upper five concentric disks with gradually decreasing radii sometime fail to form a through hole due to misalignment of the laser focus or uneven substrate surface. The bottom disks also improve the metal continuity, because they enable a smoother transition from the via to the bottom by chamfering the transition from the via to the bottom layer. The disk radii of R_1 and R_2 are chosen for the bottom disks to facilitate the alignment and fabrication, since misalignment and fabrication errors can be compensated within the larger radii R_1 and R_2. The equal via radii at the top and bottom via disks assist in the easier continuation of the layout at the top layer to the layout at the bottom layer. The radius of each circular disk is tabulated in Fig. 7(a), featuring exponentially tapered values ($r_{n+1} = e^{-1} \cdot r_n$). A Universal laser system's PLS6.75 CO_2 laser was utilized. The laser was raster-scanned over the concentric circles at 1.4 W in a speed of 71 cm/s and a resolution of 1000 pulses per inch (PPI). Five layers of silver nanoparticle ink were printed over the engraved stepped via hole using the same inkjet printing machine and settings discussed in Section II-A. The printed via sample was sintered at 120 ˚C for 2 hours. Scanning

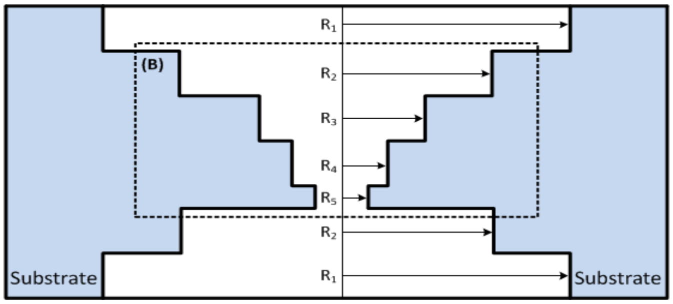

(a)

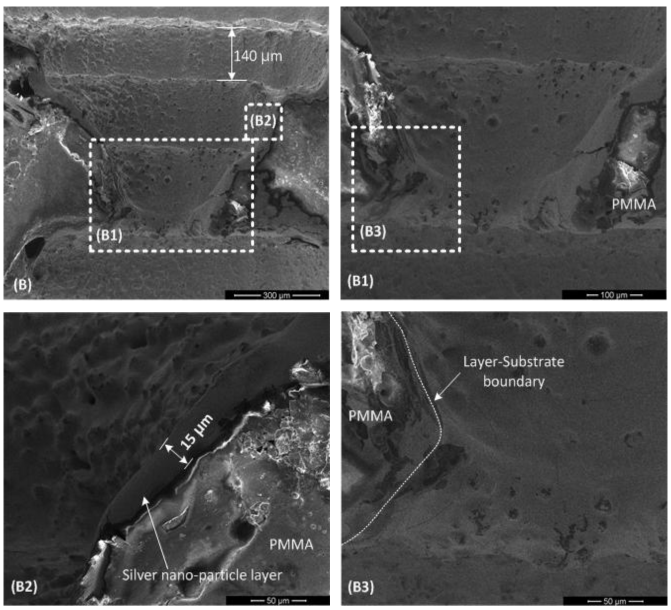

(b)

Fig. 8. (a) Geometry of stepped via hole and (b) SEM images of metalized stepped via hole: side view

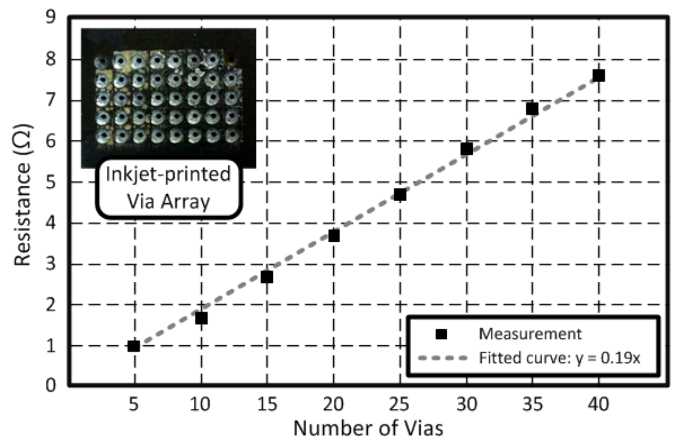

Fig. 9. Inkjet-printed stepped via array (inset) and measured DC resistance of the via chain.

electron microscope (SEM) images are shown in Fig. 7(b) and Fig. 8(b). Quanta™ 3D FEG SEM tool was utilized in this work. Fig. 7(b)-(A) shows the semicircular area of the inkjet-printed stepped via which corresponds to a dashed box in Fig. 7(a) (top view). The stepped profile of via is clearly observed with continuous metallization (Fig. 7(b)-(A)). Fig. 7(b)-(A1) ~ (A3) shows magnified SEM images of corresponding areas depicted in Fig. 7(b)-(A). Fig. 7(b)-(A1) shows a planar area of the inkjet-printed stepped via. Fig. 7(b)-(A2) shows the transition from the surface of the top substrate to the stepped via and Fig. 7(b)-(A3) shows the transition between two consecutive stepped via disks. The rough surface of the via hole is due to the laser raster scanning which utilizes a pulse laser. The profile of the stepped via hole is also shown in Fig. 8 (side view). Fig. 8(b)-(B) shows the area of the dashed boxes in Fig. 8(a). The depth of each step was around 140 µm and a continuous silver nanoparticle layer was observed throughout the entire stepped via hole. Fig. 8(b)-(B1) ~ (B3) show magnified SEM images of corresponding areas depicted in Fig. 8(b)-(B) and (B1). The silver nanoparticles form a solid layer along the via hole (Fig. 8(b)-(B2), (B3)) and a smooth transition from top to bottom is observed (Fig. 8(b)-(B3)). The transition boundary between the silver nanoparticle layer and the PMMA substrate is depicted in dashed line in Fig. 8(b)-(B3). The proposed via fabrication process is compatible with the inkjet printing technology as well as a cost efficient process since this process etches small volume of substrate material. A volume of 7-stepped via hole shown in Fig. 7 and Fig. 8 is 1.03 mm^3 while a volume of a conventional cylindrical via hole that has the same via radius of 1 mm is 3.14 mm^3. The equivalent radius of the conventional cylindrical via hole which has the same etched volume is 0.57 mm.

A via chain which consisted of 5 ~ 40 inkjet-printed stepped vias were fabricated on 0.8 mm thick Rogers RT/Duroid 5880, and the vias' DC resistance were measured to verify the repeatability and the robustness of the proposed fabrication process. The RT/Duroid 5880 was chosen to demonstrate the easy scalability of the proposed via topology, as it features low loss tangent at GHz frequency range as well as high temperature handling capability. The via chain was connected in a series. The measured resistances of the via arrays were 3.7 Ω for the 20 vias and 7.2 Ω for the 40 vias. The average resistance of the each inkjet-printed stepped via was about 0.2 Ω as shown in Fig. 9. The via resistances on PMMA and Rogers RT/Duroid 5880 are different because of substrate thickness and surface energy of the substrates. The thickness of RT/Duroid 5880 is 20 % thinner than one of the PMMA. The RT/Duroid 5880 has higher surface energy than the PMMA resulting in thicker metal trace when silver nanoparticle ink is printed.

IV. Via Modeling

A typical cylindrical via can be modeled as an inductor and a resistor in series. Circuit models for a straight cylindrical and for a generalized stepped via are in Fig. 10. The proposed stepped via can be considered as a series of cylindrical vias (Fig. 10(a)) as modeled in Fig. 10(b). The transition between the adjacent cylinders, such as D_2, D_1 and D_{n-k+1}, can be easily achieved when the both top and bottom sides are printed one by one as discussed in section III. The equivalent shunt capacitance of the stepped via is negligible when the length of the stepped via is much smaller than a wavelength at the operation frequency. For simplicity and without loss of generality, the cylinder on the bottom is chosen to have the same dimensions with the cylinders on the top as shown in Fig. 10(b)

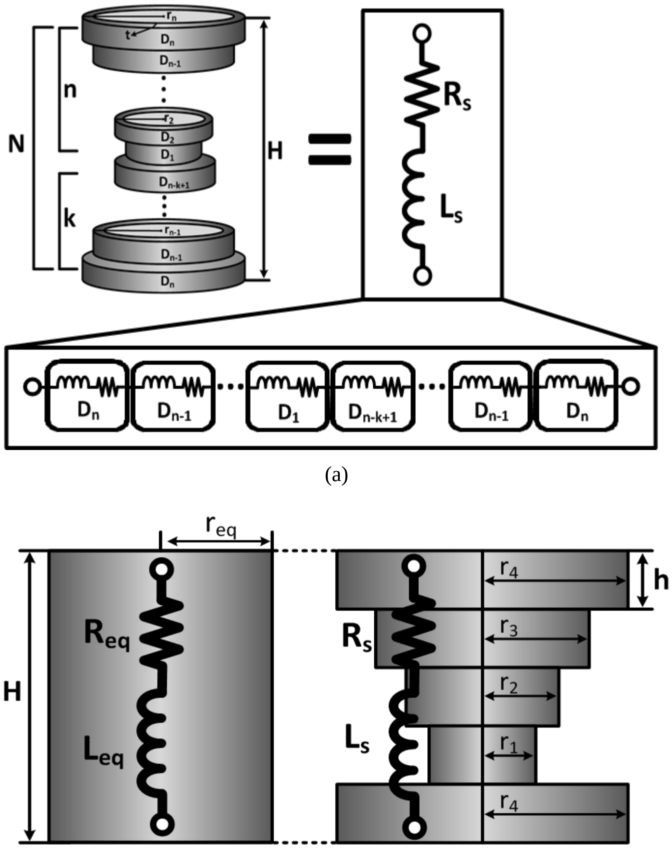

Fig. 10. (a) Equivalent circuit model of a stepped via and (b) equivalent via model of a cylindrical via and a stepped via.

and their equivalent circuit model (an inductance value and a resistance value) is derived based on the geometry of the vias. An inductance value (L_{eq}) and a resistance value (R_{eq}) of a straight cylindrical via can be expressed as shown in Eqs. (3) and (4), where the radius of the cylindrical via hole is r_{eq}, the metal thickness is t and the height of the via is H.

$$\begin{cases} L_{eq} = \frac{\mu_0 H}{4\pi} f(r_{eq}, t) \\ R_{eq} = \frac{H}{\sigma\pi} g(r_{eq}, t) \end{cases} \quad (3)$$

where

$$\begin{cases} f(r_{eq}, t) = \frac{r_{eq}^2 - (r_{eq}-t)^2 - 2(r_{eq}-t)^2 \ln\left(\frac{r_{eq}}{r_{eq}-t}\right)}{r_{eq}^2 - (r_{eq}-t)^2} \\ g(r_{eq}, t) = \frac{1}{t(2r_{eq}-t)} \end{cases} \quad (4)$$

Similarly, the circuit model (L_s & R_s) of the proposed stepped via hole can be derived based on Eqs. (3) and (4) as shown in Eqs. (5) and (6).

$$\begin{cases} L_s = \frac{\mu_0 h}{4\pi}\left[2\sum_{i=1}^{n} f(r_i, t) + \sum_{i=n-k+1}^{n} f(r_i, t)\right] \\ R_s = \frac{1}{\sigma\pi}\left[h\left(\sum_{i=1}^{n} g(r_i, t) + \sum_{i=n-k+1}^{n} g(r_i, t)\right) \quad (N = n + k, k \geq 1) \right. \\ \left. + \sum_{i=1}^{n-1} h(r_{i+1}, r_i, t) + \sum_{i=n-k+1}^{n-1} h(r_{i+1}, r_i, t)\right] \end{cases} \quad (5)$$

$$\begin{cases} f(r_i, t) = \frac{r_i^2 - (r_i-t)^2 - 2(r_i-t)^2 \ln\left(\frac{r_i}{r_i-t}\right)}{r_i^2 - (r_i-t)^2} \\ g(r_i, t) = \frac{1}{t(2r_i-t)} \\ h(r_{i+1}, r_i, t) = \frac{t}{(r_{i+1}-t)^2 - (r_i-t)^2} \end{cases} \quad (6)$$

The performance of the inkjet-printed via, such as the cut-off frequency, the inductance, and the resistance of the printed via, is a strong function of the via radius based on Eqs. (5) and (6). A via segment with a smallest radius is the most important segment of the proposed stepped-via topology since the inductance increases exponentially as the radius decreases while the resistance is inversely proportional to the via radius.

The proposed stepped via topology is easy to fabricate utilizing inkjet printing technology but it is impractical to model every different stepped via topology in full wave 3D simulators, such as HFSS and CST. It is convenient to derive an effectively “equivalent straight cylindrical via” circuit model where the composite inductance and resistance values are the same with the proposed stepped via. The 5-layered stepped via was assumed on 0.8 mm thick RT/Duroid 5880 as presented in Fig. 10 as a design example. The height of each cylinder (h) was 200 µm, the radius of the largest cylinder (r_4) was 1 mm, and the metal thickness (t) was set to 210 nm with a conductivity value of 9×10^6 S/m. The radii were exponentially increased ($r_{n+1} = e\cdot r_n$). The equivalent circuit model (L_{eq} & R_{eq}) of a cylindrical via was designed based on Eqs. (3) ~ (6). The equivalent radius (r_{eq}) of a cylindrical via was 360 µm with a metal thickness of 180 nm and a conductivity value of 1.0×10^7 S/m. Each value was calculated from the proposed equations, Eqs. (3) ~ (6). The designed equivalent circuit model of the cylindrical via has the same inductance and resistance with those values of the stepped via (L_{eq}=L_s=45.28 pH & R_{eq}=R_s=0.2 Ω). The resistance value agrees with the measurement shown in Fig. 9. The simulated equivalent via and stepped via models at microwave frequency band are shown in Fig. 11 and the results agree very well.

V. Inkjet-printed SIW Components

A SIW technology is one of the most promising technologies for high frequency applications, and numerous researches have been reported at the microwave frequency band [19]. However, there are not many reported works on printed SIW components including via metallization methods using a printing technology. The results of the inkjet-printed stepped vias and the substrate characterization at microwave frequency range suggest that relatively high conductivity values of inkjet-printed silver nanoparticles (4.6×10^6 ~ 8.0×10^6 S/m) and fabrication of numerous vias can be easily achieved. As a proof of the via fabrication concept and its application, various SIW components with large number of vias were designed, and the prototypes were experimentally investigated. Therefore, in this work, SIW structures are chosen as a design example utilizing the proposed stepped via topology to implement fully printed SIW components. In this section, a microstrip-to-SIW transition and a SIW cavity resonator are presented.

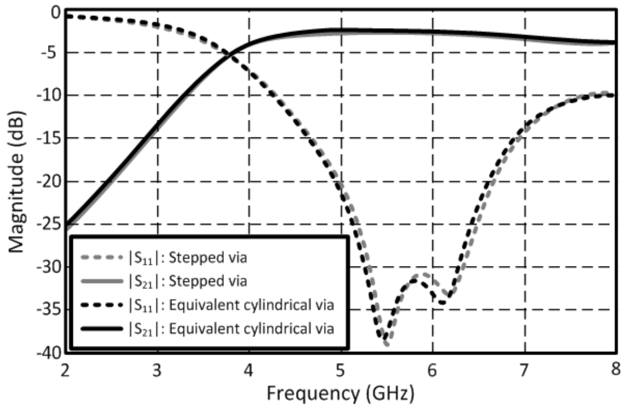

Fig. 11. Simulated S-parameters of the SIW structure with a stepped via topology and an equivalent cylindrical via topology.

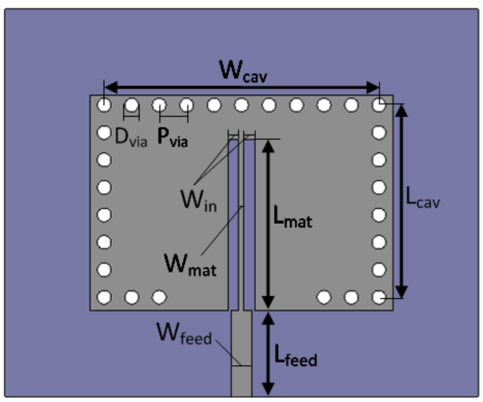

Fig. 12. Geometry of the SIW cavity resonator: W_{feed} = 2.5 mm, L_{feed} = 10 mm, W_{cav} = 32 mm, L_{cav} = 22.4 mm, D_{via} = 1.6 mm, P_{via} = 3.2 mm, L_{mat} = 17 mm, W_{mat} = 0.6 mm and W_{in} = 1.25 mm.

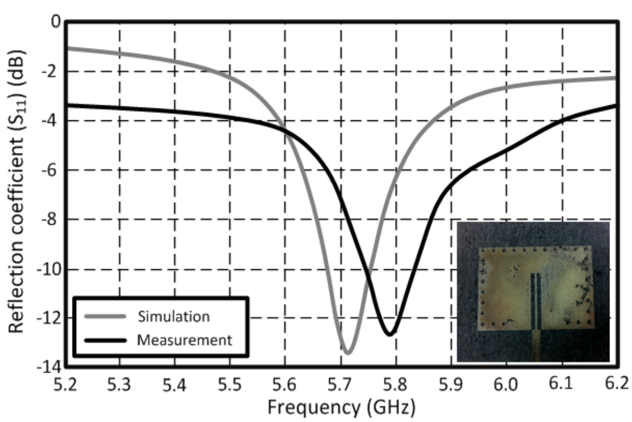

Fig. 13. Simulated and measured reflection coefficient (S_{11}) of the inkjet-printed SIW cavity resonator.

A. SIW cavity Resonator

An inkjet-printed SIW cavity resonator has been designed to verify the performance of the inkjet-printed vias. The cavity was designed to resonate at 5.8 GHz on 0.8 mm thick Rogers RT/Duroid 5880 (ε_r = 2.2, tan δ = 0.0009 at 10 GHz) in order to minimize the effect of substrate loss. The geometry of the designed SIW cavity is shown in Fig. 12. The top and bottom side of substrate were drilled utilizing a laser to form a stepped via profile as discussed in Section III. The designed pattern was printed 5 layers on top side, and a 45 mm × 40 mm patch was printed on the bottom side as a ground plane.

The measured and simulated reflection coefficients (S_{11}) are shown in Fig. 13. The results match reasonably well and their small discrepancy is due to fabrication errors stemming from the dispersion of ink on substrate after printing. The quality factor (Q-factor) of the fabricated SIW cavity is calculated using Eqs. (7)

$$Q = \frac{f_r}{\Delta f_{3dB}} \tag{7}$$

where f_r is the resonant frequency and Δf_{3dB} is the 3-dB bandwidth (half power bandwidth). The measured resonant frequency was 5.79 GHz and the 3-dB bandwidth was 0.23 GHz which results in a Q-factor of 25.13 while the simulated Q-factor was 20.05 at 5.73 GHz. The achieved Q-factor of the inkjet-printed SIW cavity was relatively low compared to the conventional cavity resonators [33,34] since the inkjet-printed metallic layer has thin metal thickness (< 5 μm) and a relatively low conductivity value compared to a bulk copper ($\sigma_{printed}$ = 9 × 10^6 S/m, σ_{cu} = 5.96 × 10^7 S/m) resulting in a high loss from metal layers.

B. Inkjet-printed Microstrip-to-SIW Transition

A simple microstrip-to-SIW transition on PMMA has been designed, and it was fully inkjet-printed by utilizing the stepped via structure for the first time. Its fundamental mode cutoff frequency (f_0) has been set to 4 GHz in order to enable an operating frequency of 5 GHz. The geometry of the proposed microstrip-to-SIW transition is shown in Fig. 14(a). Each corner of PMMA was bent due to the thermal expansion of the substrate but the middle of the SIW was flat. The SIW and the tapered transition were designed and optimized by following the reported design guide described in [35,36]. The width (W_{SIW}) and the length (L_{SIW}) of the SIW were 24 mm and 23 mm, respectively. The diameter (D_{via}) and the pitch (P_{via}) of the stepped vias were both equal to 2 mm. The length (L_{taper}) of the tapered microstrip-to-SIW transition was 12 mm and the width (W_{taper}) of it was 6 mm. The thickness of the substrate is 1 mm. Fig. 14(b) shows the fully inkjet-printed microstrip-to-SIW transition on PMMA. Vias were drilled as introduced in the Section III, and then the SIW pattern and the ground plane were printed. The printer settings and sintering temperature were the same as presented in Section II-A.

The measured and simulated values of the magnitude of the scattering parameters ($|S_{11}|$ & $|S_{21}|$) are shown in Fig. 15, demonstrating a good agreement. The measured insertion loss (IL) of the proposed microstrip-to-SIW at 5 GHz is 2.4 dB. It is notable that inkjet-printed vias have been successfully implemented.

VI. Conclusion & Future Work

In this work, the inkjet printing process of silver nanoparticles on thick substrates, such as a PMMA and RT/Duroid 5880, for microwave applications as well as the fabrication process of fully inkjet-printed low-cost vias and

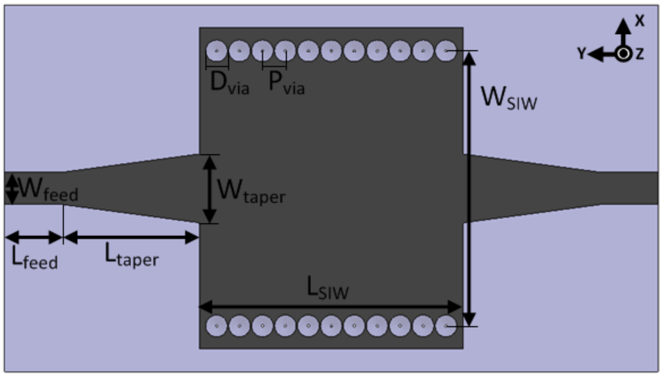

(a)

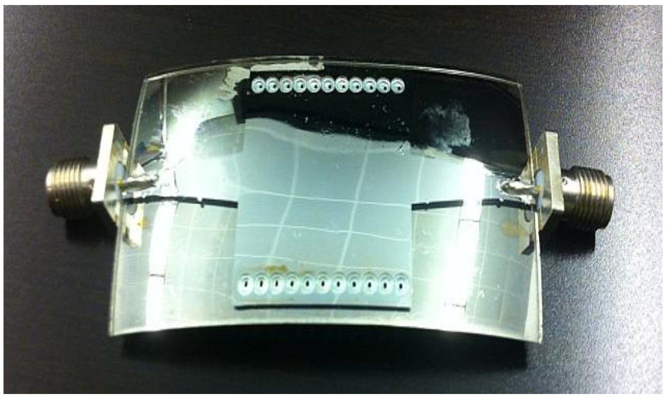

(b)

Fig. 14. MicroStrip-to-SIW transition: (a) geometry: W_{feed} = 2.8 mm, W_{taper} = 6 mm, L_{SIW} = 23 mm, W_{SIW} = 24 mm, D_{via} = 2 mm, P_{via} = 2 mm, L_{feed} = 5 mm, L_{taper} = 12 mm (b) fabricated component on PMMA.

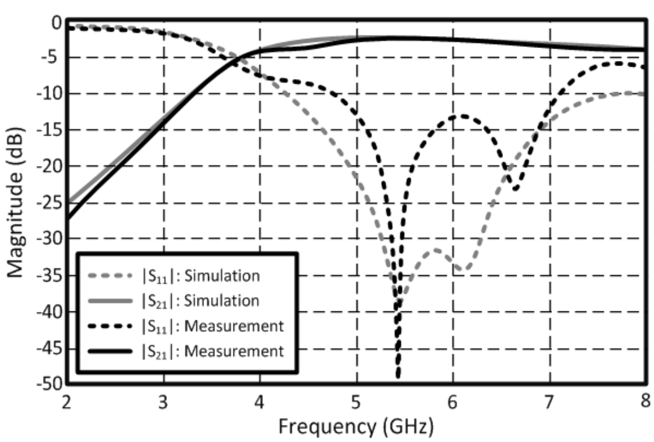

Fig. 15. Measured scattering parameters of microstrip-to-SIW transition.

SIW components are demonstrated. The inkjet-printed silver nanoparticle inks on PMMA feature good conductivity values (4.5×10^6 ~ 8.0×10^6 S/m) to implement practical microwave topologies. The fully inkjet-printed vias on the PMMA substrate were implemented by introducing a novel stepped via hole configuration with an exponentially tapered radial profile. As a proof-of-concept, fully inkjet-printed SIW structures such as a SIW cavity resonator and a microstrip-to-SIW transition were designed and experimentally demonstrated, verifying the feasibility of inkjet-printed stepped vias on various substrates.

The work presented in this paper is a fundamental study toward the future fully inkjet-printed low-cost via-enabled devices and systems including packaging. The next step of this study is to increase the thickness of the inkjet-printed silver nanoparticle films in order to reduce the skin depth effect. A proper surface treatment such as the modification of the surface energy (surface functionalization or ozone treatment), and applying mechanical constraints (increase surface roughness or implement channel for the inks) [37] could improve the printable thickness, adhesion, and uniformity of silver nanoparticles.

ACKNOWLEDGEMENT

The work of S. Kim and M. Tentzeris was supported by NSF and NEDO. The work of A. Georgiadis has been supported by the EU COST Action IC1301 WiPE Wireless Power Transmission for Sustainable Electronics, the Generalitat de Catalunya under grant 2014 SGR 1551 and by EU H2020 Marie Sklodowska-Curie grant agreement No 661621.

REFERENCES

[1] L. Atzori, A. Iera, and G. Morabito, "The Internet of Things: A survey," *Comput. Networks*, vol.54, no.15, pp.2787-2805, Oct. 2010.

[2] V. Lakafosis, A. Rida, R. Vyas, L. Yang, S. Nikolaou, and M. M. Tentzeris, "Progress Towards the First Wireless Sensor Networks Consisting of Inkjet-Printed, Paper-Based RFID-Enabled Sensor Tags," *Proc. IEEE*, vol.98, no.9, pp.1601-1609, Sep. 2010.

[3] M. Singh, H. M. Haverinen, P. Dhagat, and G. E. Jabbour, "Inkjet Printing-Process and Its Applications," *Adv. Mater.*, vol.22, no.6, pp.673-685, Feb. 2010.

[4] P. Calvert, "Inkjet Printing for Materials and Devices", *Chem. Mater.*, vol.13, no.10, pp.3299-3305, Sep. 2001.

[5] L. Yang, A. Rida, R. Vyas, and M. M. Tentzeris, "RFID Tag and RF Structures on a Paper Substrate Using Inkjet-Printing Technology," *IEEE Trans. Microw. Theory Techn.*, vol.55, no.12, pp.2894-2901, Dec. 2007.

[6] M. Mantysalo, P. Mansikkamaki, J. Miettinen, K. Kaija, S. Pienimaa, R. Ronkka, K. Hashizume, A. Kamigori, Y. Matsuba, K. Oyama, N. Terada, H. Saito, M. Kuchiki, and M. Tsubouchi, "Evaluation of Inkjet Technology for Electronic Packaging and System Integration," in *IEEE Electronic Compon. Techn. Conf.*, Reno, NV, May 2007, pp.89-94.

[7] J. -U. Park, M. Hardy, S. J. Kang, K. Barton, K. Adair, D. Mukhopadhyay, C. Y. Lee, M. S. Strano, A. G. Alleyne, J. G. Georgiadis, P. M. Ferreira and J. A. Rogers, "High-resolution electrohydrodynamic jet printing," *Nature Mater.*, vol.6, pp.782-789, Aug. 2007.

[8] M. F. Mabrook, C. Pearson, and M. C. Petty, "Inkjet-Printed Polymer Films for the Detection of Organic Vapors," *IEEE Sensors J.*, vol.6, no.6, pp.1435-1444, Dec. 2006.

[9] K. Kordás, T. Mustonen, G. Tóth, H. Jantunen, M. Lajunen, C. Soldano, S. Talapatra, S. Kar, R. Vajtai, and P. M. Ajayan, "Inkjet Printing of Electrically Conductive Patterns of Carbon Nanotubes," *Small*, vol.2, no.8-9, pp.1021-1025, Aug. 2006.

[10] S. M. Z. Hossain, R. E. Luckham, A. M. Smith, J. M. Lebert, L. M. Davies, R. H. Pelton, C. D. M. Filipe, and J. D. Brennan, "Development of a Bioactive Paper Sensor for Detection of Neurotoxins Using Piezoelectric Inkjet Printing of Sol-Gel-Derived Bioinks," *Anal. Chem.*, vol.81, pp.5474-5483, June 2009

[11] T. Kaydanova, A. Miedaner, J. D. Perkins, C. Curtis, J. L. Alleman, and D. S. Ginley, "Direct-write inkjet printing for fabrication of barium strontium titanate-based tunable circuits," *Thin Solid Films*, vol.515, no7-8, pp.3820-3824, Feb. 2007.

[12] S. Kim, A. Georgiadis, A. Collado, and M. M. Tentzeris, "An Inkjet-Printed Solar-Powered Wireless Beacon on Paper for Identification and Wireless Power Transmission Applications," *IEEE Trans. Microw. Theory Techn.*, vol.60, no.12, pp.4178-4186, Dec. 2012.

[13] S. Kim, B. Cook, T. Le, J. Cooper, H. Lee, V. Lakafosis, R. Vyas, R. Moro, A. Georgiadis, A. Collado, and M. M. Tentzeris, "Inkjet-printed

Antennas, Sensors, and Circuits on Paper Substrate," *IET Microw. Antennas Propag.*, vol.7, no.10, pp.858-868, July 2013.
[14] I. Reinhold, M. Thielen, W. Voit, W. Zapka, R. Gotzen, H. Bohlmann, "Inkjet printing of electrical vias," in *European Microelectron. Packag. Conf.*, Brighton, England, Sep. 2011, pp.1-4.
[15] T. Kawase, H. Sirringhaus, R. H. Friend, and T. Shimoda, "Inkjet Printed Via-Hole Interconnections and Resistors for All-Polymer Transistor Circuits," *Adv. Mater.*, vol.13, no.21, pp.1601-1605, Nov. 2001.
[16] T. Falat, J. Felba, A. Moscicki, and J. Borecki, "Nano-silver inkjet printed interconnections through the microvias for flexible electronics," in *IEEE Conf. Nanotechnology*, Portland, OR, USA, Aug. 2011 pp.473-477.
[17] G. McKerricher, J. Gonzalez, and A. Shamim, "All Inkjet Printed 3D Microwave Capacitors and Inductors with Vias," in *IEEE MTT-S Int. Microw. Symp. Dig.*, Seattle, WA, June 2013, pp.1-3.
[18] B. K. Terani, J. Bito, B. S. Cook, and M. M. Tentzeris, "Fully inkjet-printed multilayer microstrip and T-resonator structures for the RF characterization of printable materials and interconnects," in *IEEE MTT-S Int. Microw. Symp. Dig.*, Tampa, FL, USA, June 2014.
[19] M. Bozzi, A. Georgiadis, and K. Wu, "Review of substrate-integrated waveguide circuits and antennas," *IET Microw. Antenna P.*, vol.5, no.8, pp.909-920, June 2011.
[20] R. Moro, S. Kim, M. Bozzi and M. M. Tentzeris, "Inkjet-Printed Paper-Based Substrate Integrated Waveguide (SIW) Components and Antennas," *Int. J. Microw. Wireless Tech.*, vol.5, no.3, May 2013.
[21] Y. N. Srivastava, A.P. Gadre, T. Hylton, A. H. Monica, T. W. Schneider, R. C. White, M. Paranjape, and J. F. Currie, "Polymethylmethacrylate membrane for fluid encapsulation and release in microfluidic systems," *J. Vac. Sci. Technol. A*, vol.22, no.3, pp.1067-1072, May 2004.
[22] K. P. Latti, M. Kettunen, J. P. Stoem, and P. Silventoinen, "A review of microstrip t-resonator method in determining the dielectric properties of printed circuit board materials," *IEEE Trans. Instrum. Meas.*, vol.56, pp. 1845-1850, Oct. 2007.
[23] Y. Son, C. Kim, D. H. Yang, and D. J. Ahn, "Spreading of Inkjet Droplet on a Solid Surface with a Controlled Contact Angle at Low Weber and Reynolds Numbers," *Langmuir*, vol.24, no.6, pp.2900-2907, Feb. 2008.
[24] [Online] Available: http://www.goodfellow.com/
[25] D. Soltman and V. Subramanian, "Inkjet-Printed Line Morphologies and Temperature Control of the Coffee Ring Effect," *Langmuir*, vol.24, no.5, pp.2224-2231, Jan. 2008.
[26] T. H. J. van Osch, J. Perelaer, A. W. M. de Laat, and U. S. Schubert, "Inkjet Printing of Narrow Conductive Tracks on Untreated Polymeric Substrates," *Adv. Mater.*, vol.20, no.2, pp.343-345, Jan. 2008.
[27] J. Perelaer, B. -J. de Gans, and U. S. Schubert, "Ink-jet Printing and Microwave Sintering of Conductive Silver Tracks," *Adv. Mater.*, vol.18, no.16, pp.2101-2104, Aug. 2006.
[28] S. Kim, C. Mariotti, F. Alimenti, P. Mezzanotte, A. Georgiadis, A. Collado, L. Roselli, M. M. Tentzeris, "Perpetual RFID-Enabled Wireless Sensors for Cognitive Intelligence Applications," *Microw. Mag.*, vol.14, no.5, pp.66-77, Jul. - Aug. 2013.
[29] J. Perelaer, C. E. Hendriks, A. W. M. de Laat, and U. S. Schubert, "One-step inkjet printing of conductive silver tracks on polymer substrates," *Nanotechnology*, vol.20, no.16, Mar. 2009.
[30] R. A. Pucel, D. J. Masse, and C. P. Hartwig, "Losses in Microstrip," *IEEE Trans. Microw. Theory Techn.*, vol.16, no.6, pp.342-350, Jun. 1968.
[31] F. Declercq, H. Rogier, C. Hertleer, "Permittivity and Loss Tangent Characterization for Garment Antennas Based on a New Matrix-Pencil Two-Line Method," *IEEE Trans. Antennas Propag.*, vol.56, no.8, pp.2548-2554, Aug. 2008.
[32] H. Y. Ko, J. Park, H. Shin, and J. Moon, "Rapid Self-assembly of Monodisperse Colloidal Spheres in an Ink-jet Printed Droplet," *Chem. Mater.*, vol.16, no.22, pp.4212-4215, Oct. 2004.
[33] A. Collado, F. Mira, and A. Georgiadis, "Mechanically Tunable Substrate Integrated Waveguide (SIW) Cavity Based Oscillator," *IEEE Microw. Wirel. Compon. Lett.*, vol.23, no.9, pp.489-491, Sep. 2013.
[34] J. D. Martinez, S. Sirci, M. Taroncher, and V. E. Boria, "Compact CPW-Fed Combline Filter in Substrate Integrated Waveguide Technology," *IEEE Microw. Wirel. Compon. Lett.*, vol.22, no.1, pp.7-9, Jan. 2012.
[35] D. Deslandes and K. Wu, "Accurate modeling, wave mechanisms, and design considerations of a substrate integrated waveguide," *IEEE Trans. Microw. Theory Techn.*, vol.54, no.6, pp.2516-2526, June 2006.
[36] D. Deslandes, "Design equations for tapered microstrip-to-Substrate Integrated Waveguide transitions," in *IEEE MTT-S Int. Microw. Symp. Dig.*, May 2010, pp.704-707.
[37] C. E. Hendriks, P. J. Smith, J. Perelaer, A. M. J. van de Berg, and U. S. Schubert, ""Invisible" Silver Tracks Produced by Combining Hot-Embossing and Inkjet Printing," *Adv. Funct. Mater.*, vol.18, no.7, pp.1031-1038, Apr. 2008.

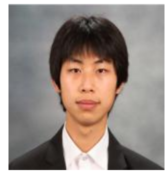

Sangkil Kim (S'12–M'15) received the B.S. degree in Electrical and Electronic Engineering from Yonsei University, Seoul, Korea, in 2010. He received the M.S. and PhD degree in Electrical and Computer Engineering from Georgia Institute of Technology, Atlanta, GA, in 2012 and 2014, respectively. He is now with Qualcomm, San Diego, CA and working on the design and analysis of inductors/transformers for high power CMOS power amplifier (PA) and LNA modules for wireless communication applications.

Atif Shamim received his M.A.Sc. and Ph.D degrees in electrical engineering at Carleton University, Canada in 2004 and 2009 respectively. He was an NSERC Alexander Graham Bell Graduate scholar at Carleton University from 2007 till 2009 and an NSERC postdoctoral Fellow from 2009-2010 at Royal Military College Canada and King Abdullah University of Science and Technology (KAUST), KSA. In August 2010, he joined the Electrical Engineering Program at KAUST, where he is currently an Assistant Professor and principle investigator of IMPACT Lab. He was an invited researcher at the VTT Micro-modules Research Center (Oulu, Finland) in 2006. Dr. Shamim was the recipient of the best paper prize at the European Wireless Technology Conference in 2008. He was given the Ottawa Centre of Research Innovation (OCRI) Researcher of the Year Award in 2008. His work on Wireless Dosimeter won the ITAC SMC Award at Canadian Microelectronics Corporation TEXPO in 2007. He received the best student paper finalist prize at IEEE APS conference in 2005. He also won numerous business related awards, including 1st prize in Canada's national business plan competition and was selected for OCRI Entrepreneur of the year award in 2010. He has authored/co-authored over 100 international publications and is an inventor on 13 patents. His research interests are in integrated on-chip antennas, low power CMOS RFICs for system-on-chip (SoC) applications and advanced system-on-package (SoP) designs in multilayer LTCC, LCP, and paper substrates through screen and inkjet printing techniques.

Apostolos Georgiadis (S'94–M'03-SM'08) was born in Thessaloniki, Greece. He received the Ph.D. degree in electrical engineering from the University of Massachusetts at Amherst, in 2002. In 2007, he joined Centre Tecnologic de Telecomunicacions de Catalunya (CTTC), Barcelona, Spain, as a Senior Researcher, where he is involved in energy harvesting and radio-frequency identification (RFID) technology and active antennas and antenna arrays. Since Apr. 2013, he is Coordinating the Microwave Systems and Nanotechnology Department at CTTC. He was the Chair of the 2011 IEEE RFID Technologies and Applications (RFID-TA) Conference. He was the Chair of EU COST Action IC0803, RF/Microwave communication subsystems for emerging wireless technologies (RFCSET) and presently he is vice-Chair of EU COST Action IC1301 on Wireless Power Transfer for Sustainable Electronics. He serves as an Associate Editor of the IEEE Microwave Wireless Components Letters, IEEE RFID Virtual Journal and IET Microwaves Antennas and Propagation journals. He is past Chair of the IEEE MTT-S Technical Committee MTT-24 on RFID Technologies and member of IEEE MTT-26 on wireless energy transfer and conversion. He is Vice-Chair of URSI Commission D Electronics and Photonics and a Distinguished Lecturer of IEEE Council on RFID (CRFID).

Hervé Aubert (M'94–SM'99) was born in Toulouse, France, in July 1966. He received the Eng. Dipl. in July 1989 and the Ph.D. degree (with high-honors) in January 1993, both in Electrical Engineering and both from the Institut National Polytechnique (INPT), Toulouse, France. Since February 2001 Hervé Aubert is Professor at INPT. He has joined the Laboratory for the Analysis and Architecture of Systems (LAAS), National Center for Scientific Research (CNRS), Toulouse, in February 2006. Since January 2015 he is the Head of the Micro- and Nano-systems for Wireless Communications Research Group at LAAS-CNRS.

From April 1997 to March 1998 he was a Visiting Associate Professor at the School of Engineering and Applied Science, University of Pennsylvania, Philadelphia, USA. He was the co-chairman of the Electronics Laboratory of INPT from July 2001 to January 2005 and the Head of the Electromagnetics Research Group of this Laboratory from July 2002 to September 2005.

Dr. Aubert has performed research work on integral-equation and variational methods applied to electromagnetic wave propagation and scattering. Currently his research activities involve the electromagnetic modelling of complex (multi-scale) structures and Wireless Sensors Networks.

Dr. Aubert has authored or co-authored one book, 2 book chapters, 75 papers in refereed journals and 200 communications in International Symposium Proceedings. He serves as an Associate Editor of Electronics Letters and he is a member of the editorial board of International Journal of Microwave Science and Technology and of International Journal of Antennas and Propagation. Dr. Aubert is the General Chairman of the European Microwave Week in 2015 (Paris, France). He is expert for the French National Research Agency (ANR) since 2009 and for the European Commission since 2012.

Manos M. Tentzeris (S'89–M'92–SM'03–F'10) received the Diploma Degree in electrical and computer engineering from the National Technical University of Athens ("Magna Cum Laude"), Athens, Greece and the M.S. and Ph.D. degrees in electrical engineering and computer science from the University of Michigan, Ann Arbor, MI, USA.

He is currently a Professor with School of Electrical and Computer Engineering, Georgia Institute of Technology (Georgia Tech), Atlanta, GA, USA. He has published more than 600 papers in refereed journals and conference proceedings, five books, and 24 book chapters. He has helped develop academic programs in highly integrated/multilayer packaging for radio frequency (RF) and wireless applications using ceramic and organic flexible materials, paper-based RFIDs and sensors, biosensors, wearable electronics, 3-D/4-D/inkjet-printed electronics, "green" electronics, energy harvesting and wireless power transfer systems, NFC systems, nanotechnology applications in RF, origami-folded electromagnetics, microwave MEMs, SOP-integrated (UWB, multiband, mmWave, conformal) antennas and heads the ATHENA research group (20 researchers). He has served as the Head of the GT-ECE Electromagnetics Technical Interest Group, as the Georgia Electronic Design Center Associate Director for RFID/Sensors research from 2006–2010 and as the Georgia Tech NSF-Packaging Research Center Associate Director for RF Research and the RF Alliance Leader from 2003–2006. He was a Visiting Professor with the Technical University of Munich, Germany for the summer of 2002, a Visiting Professor with GTRI-Ireland in Athlone, Ireland for the summer of 2009, and a Visiting Professor with LAAS-CNRS in Toulouse, France for the summer of 2010. He has given more than 100 invited talks to various universities and companies all over the world.

Dr. Tentzeris was the recipient/co-recipient of the 2015 IET Microwaves, Antennas and Propagation Premium Award, the 2014 Georgia Tech ECE Distinguished Faculty Achievement Award, the 2014 IEEE RFID-TA Best Student Paper Award, the 2013 IET Microwaves, Antennas and Propagation Premium Award, the 2012 FiDiPro Award in Finland, the iCMG Architecture Award of Excellence, the 2010 IEEE Antennas and Propagation Society Piergiorgio L. E. Uslenghi Letters Prize Paper Award, the 2011 International Workshop on Structural Health Monitoring Best Student Paper Award, the 2010 Georgia Tech Senior Faculty Outstanding Undergraduate Research Mentor Award, the 2009 IEEE Transactions on Components and Packaging Technologies Best Paper Award, the 2009 E.T.S.Walton Award from the Irish Science Foundation, the 2007 IEEE APS Symposium Best Student Paper Award, the 2007 IEEE IMS Third Best Student Paper Award, the 2007 ISAP 2007 Poster Presentation Award, the 2006 IEEE MTT Outstanding Young Engineer Award, the 2006 Asian-Pacific Microwave Conference Award, the 2004 IEEE Transactions on Advanced Packaging Commendable Paper Award, the 2003 NASA Godfrey "Art" Anzic Collaborative Distinguished Publication Award, the 2003 IBC International Educator of the Year Award, the 2003 IEEE CPMT Outstanding Young Engineer Award, the 2002 International Conference on Microwave and Millimeter-Wave Technology Best Paper Award (Beijing, CHINA), the 2002 Georgia Tech-ECE Outstanding Junior Faculty Award, the 2001 ACES Conference Best Paper Award and the 2000 NSF CAREER Award and the 1997 Best Paper Award of the International Hybrid Microelectronics and Packaging Society. He was the TPC Chair for IEEE IMS 2008 Symposium and the Chair of the 2005 IEEE CEM-TD Workshop and he is the Vice-Chair of the RF Technical Committee (TC16) of the IEEE CPMT Society. He is the founder and chair of the RFID Technical Committee (TC24) of the IEEE MTT Society and the Secretary/Treasurer of the IEEE C-RFID. He is an Associate Editor of IEEE TRANSACTIONS ON MICROWAVE THEORY AND TECHNIQUES, IEEE TRANSACTIONS ON ADVANCED PACKAGING, and the International Journal on Antennas and Propagation. He is a member of URSI-Commission D, a member of MTT-15 committee, an Associate Member of the European Microwave Association, a Fellow of the Electromagnetic Academy, and a member of the Technical Chamber of Greece. He served as one of the IEEE Microwave Theory and Techniques Society Distinguished Microwave Lecturers from 2010–2012, and he is currently serving as one the IEEE C-RFID Distinguished Lecturers.